



Degradation of sulfamethazine by biochar-supported bimetallic oxide/persulfate system in natural water: Performance and reaction mechanism



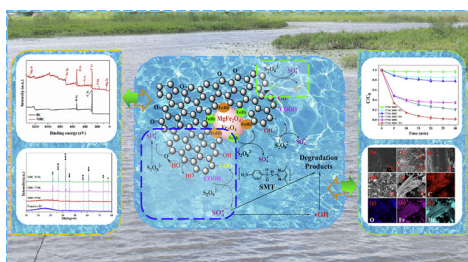
Fanzhi Qin^{a,b,1}, Yijiao Peng^{a,b,1}, Ge Song^{a,b}, Qingxuan Fang^{a,b}, Rongzhong Wang^{a,b},
Chen Zhang^{a,b,*}, Guangming Zeng^{a,b,*}, Danlian Huang^{a,b}, Cui Lai^{a,b}, Yaoyu Zhou^c, Xiaofei Tan^{a,b},
Min Cheng^{a,b}, Shiyu Liu^{a,b}

^a College of Environmental Science and Engineering, Hunan University, Changsha 410082, PR China

^b Key Laboratory of Environmental Biology and Pollution Control, Ministry of Education, Hunan University, Changsha 410082, PR China

^c College of Resources and Environment, Hunan Agricultural University, Changsha 410128, PR China

GRAPHICAL ABSTRACT



ARTICLE INFO

Editor: Xiaohong Guan

Keywords:

Biochar
Contaminated water
Sulfamethazine
Bimetallic oxide
Resource recovery

ABSTRACT

The rapid development of aquaculture results in the increased concentrations and kinds of antibiotics in water environment, and the sharply growing antibiotic contamination has caused increasing concerns. Herein, an innovative sulfamethazine (SMT) removal approach was developed by activation of persulfate (PS) using biochar-based materials prepared by co-precipitation and pyrolysis: Fe-Mg oxide/biochar (FeMgO/BC). Experiments on the activation of PS by FeMgO/BC under different factors were carried out. The involved mechanism and degradation pathway were also studied. Notably, the SMT removal rate reached 99 % under the optimum reaction condition, while the TOC removal efficiency reached 77.9 %. PS was activated by FeMgO/BC and the dominated active radical was $\text{SO}_4^{\cdot-}$. Fe^{2+} from FeMgO and the hydroxyl and carboxyl groups on the surface of biochar contributed to the production of $\text{SO}_4^{\cdot-}$. The dehydrogenation, bond cracking and unsaturated bond addition process occurred in the degradation of SMT. Furthermore, FeMgO/BC exhibits excellent reusability and stability. Considering the outstanding actual water application performances and the weak biotoxicity, FeMgO/BC shows a promising potential in the removal of antibiotics under actual water conditions.

1. Introduction

With the development of fish breeding and poultry raising,

sulfonamide antibiotics are frequently used in aquaculture and poultry industry (Zhang et al., 2016; Tian et al., 2019). During the last half century, the amount of antibiotics using by humans were about 200,000

* Corresponding authors at: College of Environmental Science and Engineering, Hunan University, Changsha 410082, PR China.

E-mail addresses: zhangchen@hnu.edu.cn (C. Zhang), zgming@hnu.edu.cn (G. Zeng).

¹ These authors contribute equally to this article.

<https://doi.org/10.1016/j.jhazmat.2020.122816>

Received 5 January 2020; Received in revised form 22 March 2020; Accepted 22 April 2020

Available online 18 May 2020

0304-3894/ © 2020 Elsevier B.V. All rights reserved.

tons worldwide (Lan et al., 2018). As a result, sulfonamide antibiotics are commonly detected in the environment (Guo et al., 2018; Li et al., 2013). What needs more attention is that sulfonamide antibiotics are difficult to be naturally metabolized in the wild (Yang et al., 2018). Therefore, residues of sulfonamide antibiotics with high environmental risks remain in aqueous environment (surface water and groundwater), soil and sediment (Wang et al., 2018; Yao et al., 2013). Sulfamethazine (4-amino-N-[4,6-dimethyl-2-pyrimidinyl] benzenesulfonamide, SMT), as one of the most representative and effective antibiotics, was used widely in the treatment and prevention of influenza (Huang et al., 2019). However, the accumulation and enrichment of antibiotics such as SMT in the environment will induce the genetic mutation of pathogenic bacteria and enhance the drug resistance of bacteria. More seriously, the transmission of antibiotics through food chains will lead to some human diseases facing the dilemma of no effective drug treatment. Therefore, it is critical and crucial to study and find a more efficient way to remove sulfonamide antibiotics from wastewater (Huang et al., 2017a; Yin et al., 2019).

Biochar, a fascinating environmental restoration material, has caught the attention of many researchers due to its excellent physical properties and economic practicality (Zhang et al., 2019a, b). Biochar can be prepared by pyrolysis of organic wastes and various biologic materials (Yang and Sheng, 2003). Compared with clay minerals (Gao and Pedersen, 2005) and nano materials (Lai et al., 2018; Chen et al., 2015), taking cost and efficiency into consideration (Huang et al., 2017b, c), biochar is regarded as an important alternative for wastewater treatment because of its high specific surface area (Gong et al., 2017), multiple binding sites and lower price (Huang et al., 2017c, 2016). However, biochar materials are insufficient for the removal of SMT due to the limited adsorption capacity and extremely weak degradation capacity (Waclawek et al., 2016). The combination of adsorption and degradation towards antibiotics has attracted increasing interests (He et al., 2019).

Advanced oxidation processes (AOPs) based on free radicals have been investigated by researchers towards antibiotic contaminations. It is promising to combine AOPs with biochar amendment (Hu et al., 2018; Yang et al., 2019a). Among all free radicals, such as hydroxyl radical ($\cdot\text{OH}$), superoxide radical ($\cdot\text{O}_2^-$), carboxyl radical ($\cdot\text{OOH}$) and sulfate radical ($\text{SO}_4^{\cdot-}$), $\text{SO}_4^{\cdot-}$ shows more competitive advantages because it owns a higher redox potential (2.5-3.1 V) than $\cdot\text{OH}$ (1.9-2.7 V) and shows better performance in a wide range of pH (Zeng et al., 2015). Therefore, PS activation can improve the degradation speed of highly toxic and persistent pollutants, e.g., hexachlorocyclohexanes, antibiotics and pharmaceuticals (Waclawek et al., 2016). Naturally, the activation of PS to produce $\text{SO}_4^{\cdot-}$ has become an important research topic. Li et al. studied the generation of $\text{SO}_4^{\cdot-}$ through pyrolytic activation (Li et al., 2013). And transition metals and base-activation were also reported (Yin et al., 2019). However, when Fe^{2+} works during the activation of PS, the excessive heavy metal leaching remains risk of secondary contamination, thus restricting its application prospect (Muhammad et al., 2012). Hence, a stable, efficient and economical method for PS activation is urgently needed, and applications in real water samples should get more discussion and research.

The large specific surface area, sophisticated porosity and wide range of feedstocks make biochar a considerable choice to load target particles and synergistically work with PS (Chen et al., 2018; Cheng et al., 2017). Fe_3O_4 has been applied in Fenton or Fenton-like process, which has stable spinel lattice and shows a high magnetic behavior. Zhang et al. combined Fe_3O_4 and biochar for dyeing wastewater treatment (Zhang et al., 2018). Meanwhile, biochar modified with MgO shows remarkable performance in phosphate and nitrate removal with highly available binding sites (Jung and Ahn, 2016; Zhang et al., 2012). Thus, magnesium ferrite with spinel lattice (MgFe_2O_4) comes into researchers' sight (Zhou et al., 2018). Compared with Fe_3O_4 , MgFe_2O_4 has lower price of raw materials and can effectively reduce secondary pollution released by Fe. Therefore, combining biochar with Fe-Mg

oxide (FeMgO) containing Fe_2O_3 , MgFe_2O_4 and MgO , is very promising due to the excellent adsorption capacity of biochar (Khot et al., 2012) and the catalytic activity of FeMgO for producing $\text{SO}_4^{\cdot-}$ (Jung et al., 2017). Moreover, functional groups on biochar can also contribute to the activation of PS (Wang et al., 2017). However, the investigation on FeMgO/BC for the activation of PS has seldom been reported, especially in the actual water application.

In this work, a practical and eco-friendly method to synthesize biochar-based magnetic materials was proposed. Material characterizations were conducted to test material properties, including surface morphology, pore size distribution, specific surface area, functional groups, and element composition. Experiments have been conducted to test the effect of PS activation and optimize SMT removal conditions. More importantly, in order to study the degradation pathway of SMT, the intermediates and degradation products were analyzed and toxicity experiment was also carried out. Free radical scavenging experiment and ESR analysis were used to determine the dominated free radicals and the involved mechanisms. Finally, the reutilization and stability of the material have been tested, and experiments of practical application in different natural water systems were also investigated.

2. Materials and methods

2.1. Materials

SMT was bought from Sinopharm Chemical Reagent Co., Ltd. Its physicochemical properties such as the molecular structure, $\lg K_{ow}$, acid dissociation constant and water solubility were shown in Table S1. Ammonium persulfate, ferric trichloride hexahydrate and magnesium chloride hexahydrate were also purchased from Sinopharm Chemical Reagent Co., Ltd. Except the maize straw and sulfamethazine, all chemicals were analytical grade. The water for dilution and dissolution was ultrapure water (resistivity of 18.25 M Ω cm).

2.2. Preparation of FeMgO/BC

The FeMgO/BC composite was prepared as follows: 5 g of maize straw powder was added into 100 mL ultrapure water, vibrating at a speed of 200 rpm for 30 min in constant-temperature water bath shaker. 0.4 M magnesium chloride hexahydrate and 0.8 M ferric trichloride hexahydrate were added into the system and continued to react for 4 h at 333 K to get the suspension via co-precipitation method. The suspension was centrifuged, and the obtained solid mixture was washed with ultrapure water, then dried at 333 K for 24 h to get the raw materials (Jung et al., 2017). The treated raw materials were pyrolyzed at 573 K, 773 K and 973 K under nitrogen atmosphere, respectively. The heating rate was 8 K/min, and the final materials were obtained after pyrolyzing for 2 h and cooling to room temperature. All biochar/magnesium ferrite (FeMgO/BC) were ground and sifted by 100 mesh sieves for later use. For a comparative analysis, through the same process, pristine biochar and FeMgO particles were also prepared.

2.3. Characterization of materials

The surface area and pore distribution of biochar and FeMgO/BC were measured through Brunauer-Emmett-Teller (BET) surface area measurement (Micromeritics, ASAP 2020, USA). The surface microstructure of prepared material was analyzed by field emission scanning electron microscope (FESEM, Hitachi SU8220). X-ray diffraction (XRD, Bruker AXS D8 Advances) was used for analyzing the composition of the prepared materials. Vibrating sample magnetometer (VSM, MPMS-XL-7, America Quantum Design) was utilized to measure the magnetic properties of the material. X-ray photoelectron spectroscopy (XPS, ESCALAB 250Xi, Thermo Fisher) and electron spin resonance (ESR, JES-FA200, JEOL) were used to study the fresh materials and used materials. Analysis of complex organic compounds was carried out by

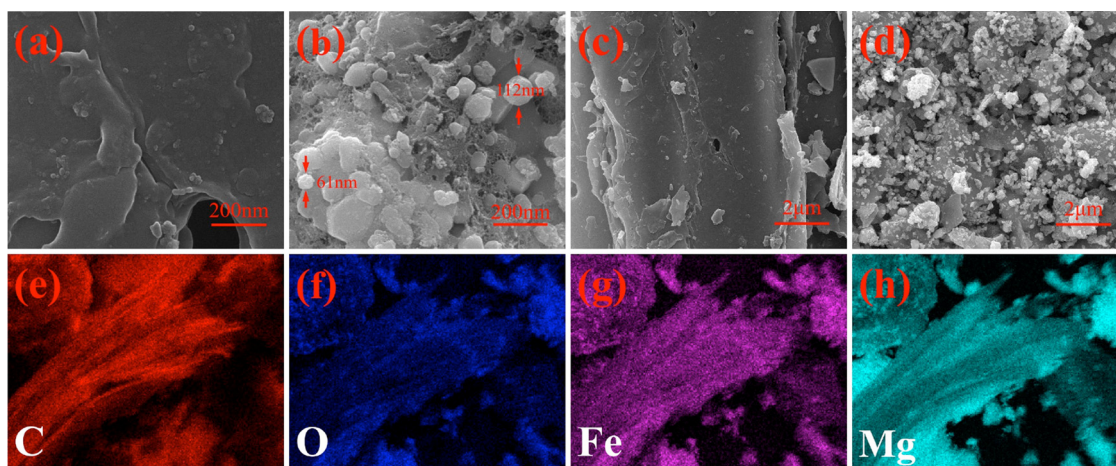


Fig. 1. SEM images of materials' morphology property and composition: (b, d) modified biochar (BC) and (a, c) original biochar (BC); (e, f, g, h) EDS elemental mapping images of MBC.

liquid chromatography-triple quadrupole mass spectrometer (LC-MS, 6470 Triple Quad, Agilent).

2.4. Persulfate activation

Batch tests were carried out in 20 mL glass bottle containing SMT, PS and prepared materials. 100 mg/L SMT and 40 mM of PS were prepared for further dilution. The single-variable control trials were conducted in order to study and optimize the removal conditions including initial pH, PS concentration, material dosage, temperature and reaction time. The pH values were adjusted by hydrochloric acid and sodium hydroxide, then fixing it in the constant-temperature water shock chamber at 170 r/min and 298 K, shaking for 1 h, and finally using the filter (0.45 μm PTFE disposable filters) to filter the liquid mixtures. The concentration of SMT in the sample was determined by high performance liquid chromatograph.

2.5. Mechanism and degradation pathway study

A series of comparative analysis was conducted on the active sites of biochar and the role of supported FeMgO in the activation of PS. The changes of BC and FeMgO/BC were characterized by XPS and other characterization methods. To determine the kind of free radical dominating in the process of SMT degradation, the comprehensive analysis of the free radical quenching experiment and ESR characterization were conducted. Particularly, Methanol ([MeOH] = 1.85 M), tert-butanol ([TBA] = 1.85 M) and p-benzoquinone ([PBQ] = 2 mM) were added into the reaction system as free radical scavengers. In order to explore the process of catalytic oxidation and propose a reasonable SMT degradation route, the analyses of SMT chemical structures and the intermediate products corresponding to standard mass spectrometry were carried out.

2.6. Toxicity assessment test

The toxicity of reaction solution during treatment was evaluated with traditional bacterial growth. Gram-negative strain *Escherichia coli* (*E. coli*) was selected as a model bacterium for testing. The viable cell density of the *E. coli* stock suspension for the experiment was 2.0×10^7 CFU/mL. The glass instruments, deionized water and Eosin Methylene Blue Agar nutrient solution were all sterilized at 394 K for 20 min in a vertical pressure steam sterilizer. Typically, 10 μL of bacterial stock solution (2.0×10^7 CFU/mL) was added into 990 μL of SMT reaction solution sampled at given time intervals during the reaction process (SMT solution treated with FeMgO/BC). The mixed solution was kept in

a biochemical incubator (310 K) for 1 h, then diluted with sterilized water and spread on Eosin Methylene Blue Agar plate. Thereafter, the treated agar plate was incubated at 310 K for 24 h. The viable cell density of each sample was measured by standard plate count method. The control experiment was carried out by adding the sterilized water instead of the reaction solution.

2.7. Removal performance of FeMgO/BC in different natural water samples

For the removal study in actual water systems, samples from Xiangjiang river (Changsha), the lake water from Peach Lake (Changsha), the pond water from the Niuxin Pond and Xichong Pond, as well as tap water (Changsha Running-water Company) and ultra-pure water were used. An appropriate amount of FeMgO/BC and PS were added, and the concentration of SMT was designed to be 30 mg/L. The total organic carbon was measured by TOC analyzer.

2.8. Stability test of FeMgO/BC

XPS characterizations of FeMgO/BC before and after the reaction were carried out, and iron and magnesium leaching experiments were conducted to comprehensively analyze the changes of surface elements during oxidation process. In order to study the reusability of the material, repeated use of the same material to remove SMT were performed. The conditions for each test were controlled as follows: reaction time = 1 h, system volume = 30 mL, [SMT] = 30 mg/L, material dosage = 2 g/L, [PS] = 5 mM, pH = 3, T = 298 K. After the use of FeMgO/BC, magnet was used to separate the material and 0.5 M NaOH was used for desorption. The residual NaOH was cleaned by suction filtration with ultrapure water. The separated FeMgO/BC was dried in thermostatic drier box for 24 h and then used in the next recycle.

3. Results and discussion

3.1. Characterization of BC and FeMgO/BC

The initial biochar (BC) and modified biochar (MBC) were analyzed by SEM for observing the microscopical surface morphology and the loading status. It can be obtained from Fig. 1 that the biochar existed in the form of flake, while the supporting substance existed in the state of spheroid. The maximum particle size was about 110 nm, and the uniform and dense distribution of the loaded particles reflected a good distribution. The BET surface area increased from 68.71 m²/g to 256.58 m²/g after FeMgO loading, while the pore size decreased from 9.92 nm to 2.04 nm. These data indicated that the material was a mesoporous

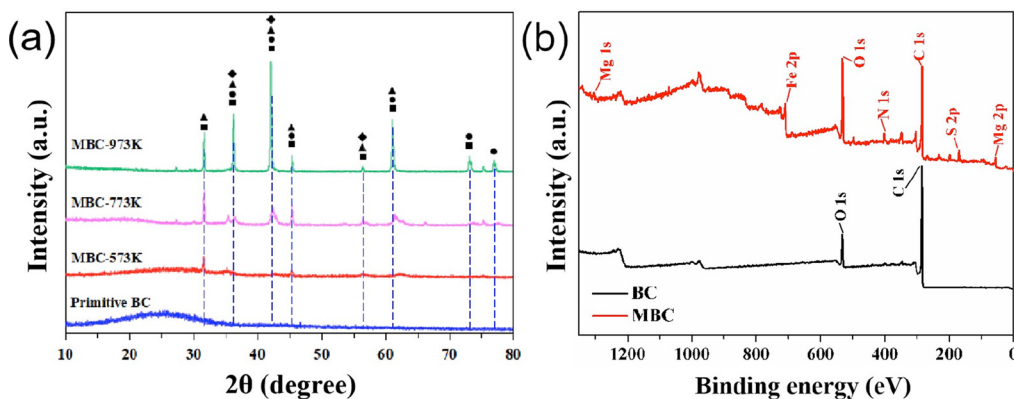


Fig. 2. (a) XRD pattern of primitive biochar (BC) and modified biochar (MBC) under 573 K, 773 K and 973 K. And (■), (◆), (▲) and (●) represent MgFe_2O_4 , Fe_3O_4 , $\gamma\text{-Fe}_2\text{O}_3$ and MgO , respectively; (b) XPS spectra of MBC and BC.

material with good adsorption capacity, and the loading of FeMgO greatly enlarged the material surface area. The results of mapping imagines in Fig. 1 show that Fe, Mg, O and C were uniformly distributed with high element content on the surface of the material, suggesting the good loading condition. The SEM diagram corresponding to the mapping images was shown in Fig. S1.

XRD spectra of MBC and BC were shown in Fig. 2b, which indicated that Fe and Mg appeared on the composite and the ratio of oxygen increased. In order to investigate whether metal-O-C bonds were successfully formed, the characterization of XPS on O 1s was carried out on BC and MBC (Fig. 3 and Table 1). According to previous literatures, C-O and C = O peaks centered at 533.2 eV and 531.2 eV, while 531.8 eV and 530.3 eV were attributed to Fe-O-C and Fe-O bonds, respectively (Zhou et al., 2011; Xiao et al., 2016). As can be seen from the Fig. 3, MBC had two more peaks representing Fe-O-C and Fe-O, which indicated that iron was firmly bonded to biochar in the form of chemical bond force. The characterization of XPS on C 1s was also carried out on

Table 1

Proportion of different kinds of bonds in BC and MBC.

Sample	C-C	C-O-C/C-OH	O=C-O	C=O	$\pi\text{-}\pi^*$
BC	61.57%	34.62%	0.93%	2.36%	0.52%
MBC	52.25%	38.72%	1.35%	7.19%	0.50%

MBC, and the data obtained from the experiment were shown in Fig. 3, which indicated the presence of $\text{C}=\text{C}$ and $\text{CO}=\text{}$. Two conclusions could be drawn: i) after loading with bimetallic oxides, the carboxyl and hydroxyl groups increased, and ii) aromaticity of the materials represented by $\pi\text{-}\pi^*$ showed no significant change, which was beneficial to improve the removal efficiency of SMT.

The original biochar and composites produced by pyrolysis at three different temperatures were analyzed with XRD to investigate the internal structure of the materials. ICDD cards were used for comparative

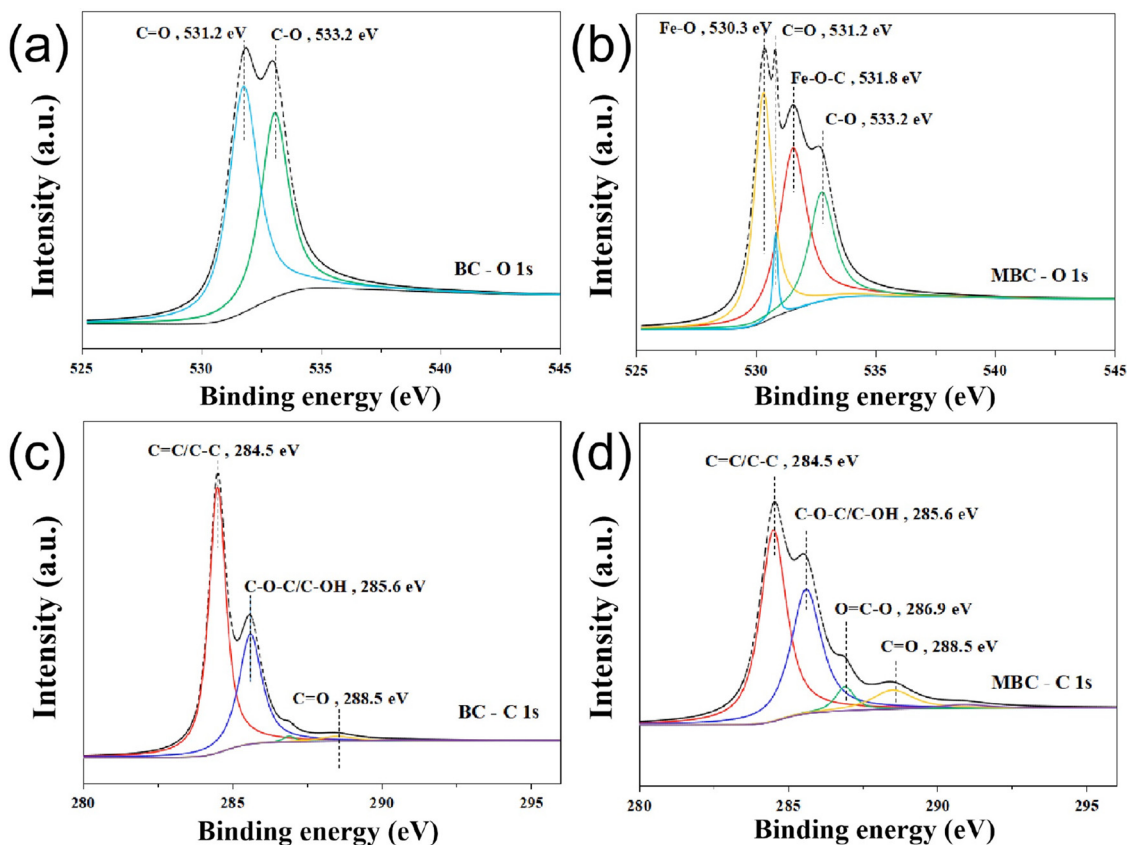


Fig. 3. Deconvolution of XPS C 1s and O 1s for BC and MBC.

analysis, and the results of the analysis was presented in Fig. 2a and it was found that the synthesized materials mainly contained MgFe_2O_4 and MgO (Kohsari and Norouzbeigi, 2018). Notably, diffraction peaks at 35.5° and 43.2° (2 θ) indicate the existence of Fe_3O_4 , which released Fe^{2+} during the reaction for activating PS. The increase of peak sharpness and no significant change of peak width indicated that the crystallinity improved with the increase of temperature, and there was a weak sharp peak at a high angle. Equally important, the presence of more spinel crystals in materials obtained at 973 K represented a prominent increase in the magnetic properties of the material (Tang et al., 2013). Fig. 2a also showed that the diffraction angle become more obvious and sharper with the increase of temperature, which may be due to the removal of water, including crystal water and free water. The increase of MgO and Fe_2O_3 strengthened the solid state reaction between them and produced more MgFe_2O_4 with spinel type (Bououdina et al., 2019). The magnetic properties of materials were analyzed by using magnetic regression curves (Fig. S2), which showed that the saturation magnetization values of the material before reaction and after reaction were 35.25 emu/g and 37.55 emu/g, respectively. The high saturation magnetization value is conducive to the rapid separation of the material under the action of external magnetic field, which is also confirmed by the illustration in Fig. S2. In accordance with the above analysis, MgFe_2O_4 and Fe_3O_4 mainly contribute to the magnetism of FeMgO (Jung et al., 2017).

3.2. Catalytic performance of FeMgO/BC

Experiments were carried out to study the effect of different materials on SMT removal, including BC and MBC. Each result was based on three parallel experiments whether PS added or not. The TOC removal efficiencies of different materials were compared, including PS, FeMgO , FeMgO/PS , BC, BC/PS, MBC, MBC/PS, and the blank control group. As shown in Fig. S3, the MBC/PS system achieved the best TOC removal efficiency, up to 78 %. It was worth noting that the TOC removal efficiency for bimetallic oxides was poor, even worse than that of biochar. This could be due to the difficulty for the FeMgO to disperse evenly without the support of biochar, and the synergistic effect between biochar and FeMgO didn't exist (Jung et al., 2017). Comparing the SMT removal efficiency in Fig. 4a, the efficiency of FeMgO/BC was 48 % higher than and that of BC (with or without PS), which was consistent with the BET results. Notably, in the reaction system contained FeMgO/BC and PS, the removal rate was significantly higher than others. This experimental result indicated that the PS was successfully activated in the reaction system. In order to further determine the relationship between the dosage of added material and removal efficiency, the initial dosage of FeMgO/BC was set at 0.5, 1.0, 2.0, 3.0, 5.0, and 10.0 g/L, respectively. It could be observed from Fig. 4b that when the dosage of FeMgO/BC increased from the initial 0.5–2.0 g/L, the SMT removal

efficiency remarkably increased. However, after the initial material addition exceeded 2.0 g/L, the increment increased slightly, which might be due to the residual SMT and the dispersed distribution (Lin et al., 2016; Barhoumi et al., 2016). Another possible reason was that FeMgO/BC released too much Fe^{2+} reacting with hydroxyl radicals (Yan et al., 2016), thus reducing the free radical content. Therefore, 2.0 g/L is the best catalyst dosage for SMT removal.

Fig. 5(a) shows that the reaction equilibrium was reached within 30 min, which might be due to the increase of adsorption sites on the surface of biochar and the advanced oxidation process brought by PS (Sun et al., 2018). In previous literatures, electrostatic force, π - π interactions, and hydrogen bonds are the main force when biochar composites interact with antibiotics in water (Teixidó et al., 2011). In the initial stage of contact, the high concentration of antibiotics in the solution and the low concentration on the uncovered adsorbent surface formed a favorable concentration gradient, which was conducive to promoting the mass transfer of SMT (Mohammadi et al., 2011). The Fig. 5a showed that the adsorption capacity of FeMgO/BC prepared at 973 K was higher than those prepared at the other two different temperatures. It might be because the increase of pyrolysis temperature could lead to the increase of aromatization of the composites (Chen et al., 2008). At the same time, the continuous increase in temperature also improved the pressure inside the material, resulting in the fracture and recombination of the internal structure of the material (Yang et al., 2019a; Ahmad et al., 2014). In addition, the influence of temperatures on the SMT removal process was also investigated at four temperatures. Fig. S4 clearly shows that the removal efficiency of SMT increased significantly with the increase of temperature. This conclusion may due to the affinities of the binding site and the synergistic effect of MBC and PS improved with the increase of temperature (Jung et al., 2017; Matzek and Carter, 2016).

The solution pH affects the charge of the surfaces of both the composites and the form of SMT (Zhang et al., 2011). Five pH values ranging from 3 to 11 were set at intervals of 2 to study the effect of pH. In previous studies of our group (Fig. S5), the speciation distribution of SMT varied depending on pH. When pH is around 3, SMT mainly exists in the form of positive charge, and when pH is more than 7, SMT has the highest distribution coefficient, and when pH is about 5, most target pollutant particles are in the neutral state (Zhang et al., 2016; Ling et al., 2016). Fig. 6a shows that the best removal efficiency appeared when pH value was 3, which might be attributed to i) the protonated SMT in the acidic environment, which was in good agreement with the charged properties of the composite surface (Li et al., 2016) and ii) when pH is too high, both $\cdot\text{OH}$ and SO_4^- were consumed in the chemical reactions resulting in the reduction of removal efficiency (Lau et al., 2007). As presented in Fig. 6, when the experimental conditions were $[\text{SMT}] = 5 \text{ mg/L}$ and $[\text{PS}] = 5 \text{ mM}$, the highest removal efficiency reached 99.8 %.

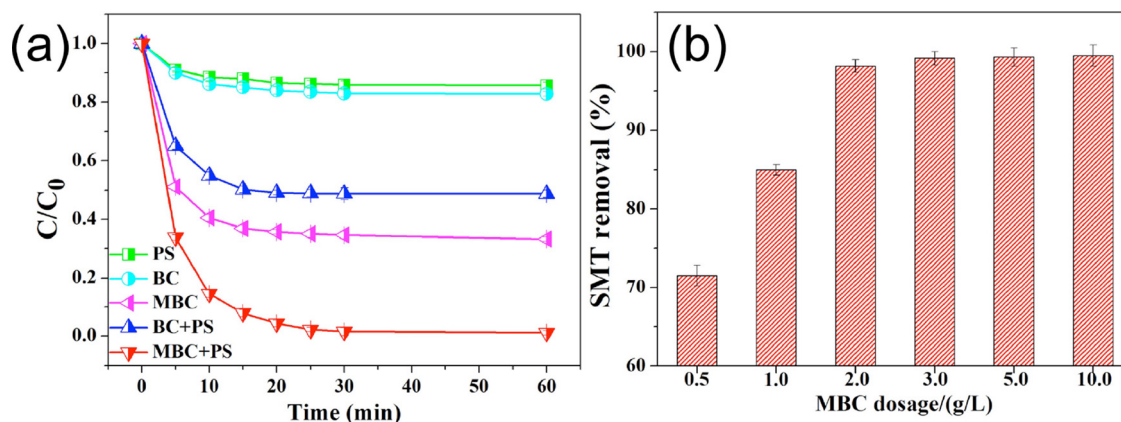


Fig. 4. Removal amount of sulfamethazine with different materials (a) and different dosage (b).

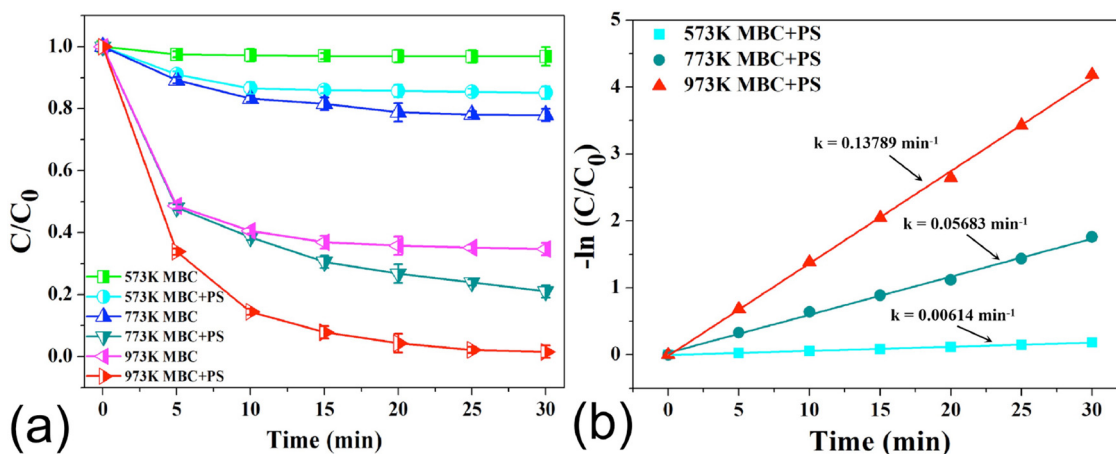


Fig. 5. Relationship between removal rate and time (a), which represents the material alone and the synergistic action with PS. The first-order kinetic fitting results (b) for materials pyrolyzed at 573 K, 773 K and 973 K.

Fig. 6b also proves that biochar-supported bimetallic oxide/PS is an efficient and practical activation system, especially, when the initial SMT concentration was high, such as $[SMT] = 50 \text{ mg/L}$, and the removal amount of SMT significantly increased with the increase of PS concentration. However, when the concentration of SMT was low, the addition of PS did not significantly contribute to the increase of SMT removal rate, which might be attributed to the adsorption properties of the composites. Moreover, when PS concentrations were higher than 5 mM, the removal rate of SMT did not change significantly even at different SMT concentrations. One reason is that the total removal is close to saturation and another factor is that chemical reactions take place between $\text{SO}_4^{\cdot-}$, and the resulting $\text{S}_2\text{O}_8^{2-}$ react with $\text{SO}_4^{\cdot-}$ again, leading to a significant drop of the $\text{SO}_4^{\cdot-}$ concentration (Liang et al., 2004; Yang et al., 2019b). Therefore, option of $[PS] = 5 \text{ mM}$ can achieve a high removal efficiency.

3.3. Identification of the dominant radicals

Free radical quenching experiments and ESR analysis were conducted to explore the types of free radicals that had redox reactions with SMT and their contribution proportion in the removal process. [DMPO] was used as the spin trapping agent in the ESR process capturing $\cdot\text{OH}$ and $\text{SO}_4^{\cdot-}$ effectively. It could be seen from the spectrum (Fig. 7a) that with the increase of the reaction time, the concentration of corresponding free radicals in the system of biochar or composites all increased. The peak shape in Fig. 7b indicated that $\cdot\text{O}_2^-$ production was achieved in 20 min, which was consistent with the formation of $\cdot\text{OH}$ and $\text{SO}_4^{\cdot-}$. Compared with biochar, the free radical abundance in

the system of composites was significantly higher, which also proved that the supported particles successfully activated PS. In this process, $\cdot\text{OH}$, $\text{SO}_4^{\cdot-}$ and $\cdot\text{O}_2^-$ were produced and participated in the degradation process of SMT.

Particularly, free radical quenching experiments were conducted to investigate the dominant free radical. Methanol ($[\text{MeOH}] = 1.85 \text{ M}$), tert-butanol ($[\text{TBA}] = 1.85 \text{ M}$) and p-benzoquinone ($[\text{PBQ}] = 2 \text{ mM}$) were added into the reaction system as free radical scavengers. The different reaction constants of the quenching agents are listed in Table S3. In terms of scavenging $\cdot\text{OH}$ and $\text{SO}_4^{\cdot-}$, MeOH obviously has excellent performance for both $\cdot\text{OH}$ and $\text{SO}_4^{\cdot-}$, while TBA shows poor ability for scavenging $\text{SO}_4^{\cdot-}$. When the concentration of MeOH was 1.85 M, the degradation efficiency of SMT was 52.47 %, when the removal percentage of the control group with was 98.06 %. In the presence of $[\text{TBA}] = 1.85 \text{ M}$, the removal percentage of SMT decreased to 90.83 %, and it was 7.23 % lower than that of the control group, and 38.36 % higher than that of the group with scavenger MeOH. Besides, the addition of PBQ, which is capable of scavenging $\cdot\text{O}_2^-$, was also carried out. The results showed that $\cdot\text{O}_2^-$ also played a role in the degradation of SMT, which was probably due to that the oxygen in the water captured the electrons (Furman et al., 2010). Through the data presented in Fig. 8, it could be concluded that both $\cdot\text{OH}$ and $\text{SO}_4^{\cdot-}$ all contributed to the reaction with SMT during the degradation process, but obviously, $\text{SO}_4^{\cdot-}$ played the dominated role.

3.4. Intermediates analyses and the proposed transformation pathways

Based on the analysis of intermediates produced during the SMT

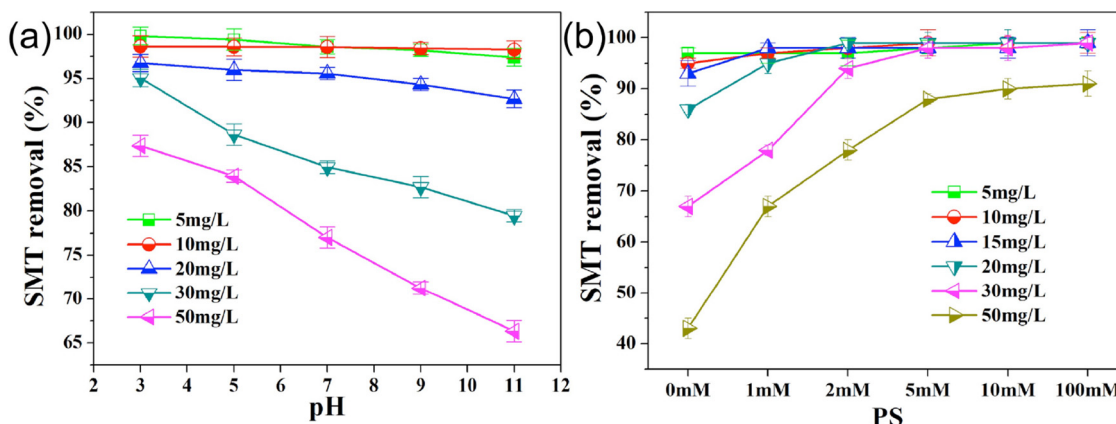


Fig. 6. Degradation of sulfamethazine at different conditions. Different pH values (a) and different concentrations of PS (b) with SMT at 5, 10, 20, 30 and 50 mg/L.

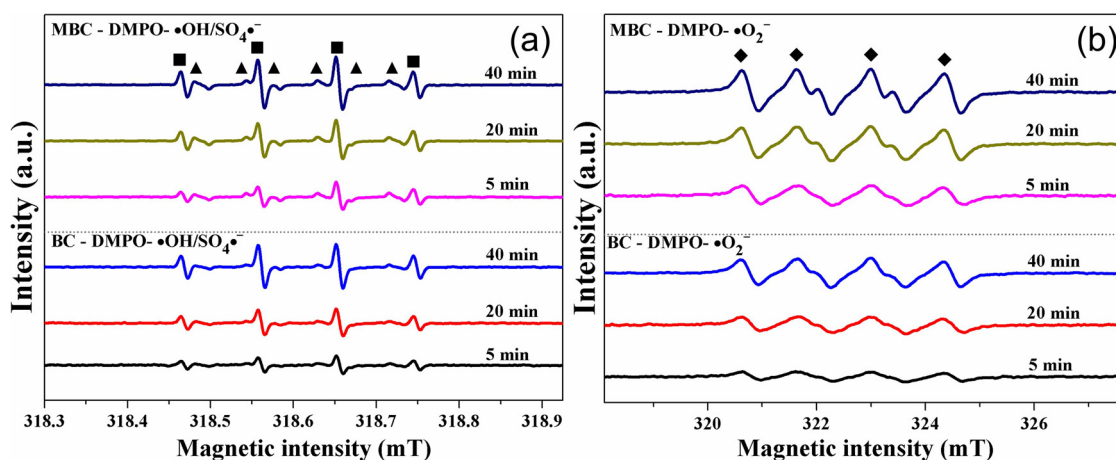


Fig. 7. Identification of dominated free radicals. ESR results of (a) $\bullet\text{OH}$ (■), $\text{SO}_4^{\bullet-}$ (▲) and (b) $\bullet\text{O}_2^-$ (◆) trapped by DMPO at leaching time for 5, 20 and 40 min.

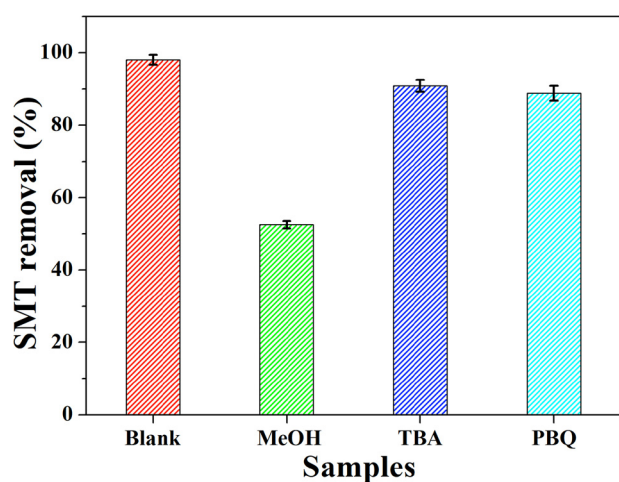


Fig. 8. Quenching results of different free radical scavengers.

Table 2
Relevant intermediates reported by LC-MS spectra of SMT degradation.

Compound	t_r (min)	Molecular structure	Molar Mass (g mol ⁻¹)
A 4-aminobenzenesulfonic acid	8.35		173
B 4-(hydroxyamino) benzenesulfonic acid	2.78		189
D 4-aminophenol	1.42-1.44		109
E 4,6-Dimethyl-2-pyrimidinamine	1.73		123
F 2-(hydroxyamino)-4,6-pyrimidine dicarboxylic acid	1.42-1.44		199
G 2-amino-6-methylpyrimidine-4-carboxylic acid	1.42-1.44		153

degradation process with LC-MS, evidences of the existence of several stable organic molecules have been obtained, which are shown in Fig. S7. Combined with previous literature analyses, the products are summarized in Table 2. A possible SMT degradation pathway is proposed through a comprehensive analysis of the detected species (Fig. 9).

Two of the most important parts in the mineralization of SMT are the initial cleavage of the sulfonamide N-S bond and the opening of the benzene ring and the nitrogen-containing heterocyclic ring (Barhoumi et al., 2016). The former is caused by the attack of $\bullet\text{OH}$ and/or $\text{SO}_4^{\bullet-}$, producing 4-aminobenzenesulfonic acid (A) and 4,6-dimethyl-2-pyrimidinamine (E). Due to the function of free radicals, a continual oxidation reaction of 4-aminobenzenesulfonic acid (A) happens, yielding 4-(hydroxyamino) benzenesulfonic acid (B) and hydroxylated 4-(hydroxyamino) benzenesulfonic acid (1:1) (C). After desulfonation reaction, bonds of (B) and (C) break again and 4-aminophenol (D) is generated. Further oxidation of 4,6-dimethyl-2-pyrimidinamine (E) produces 2-(hydroxyamino)-4,6-pyrimidine dicarboxylic acid (F) and 2-amino-6-methylpyrimidine-4-carboxylic acid (G) (Zhou et al., 2014). Nitrogen and sulfur elements contained in SMT exist in the form of inorganic ions after complex ring-opening reactions, such as SO_4^{2-} , NH_4^+ and NO_3^- (Zhou et al., 2014). Fig. S7 showed that the amount of organic matters reached the maximum at 10 min. With the progress of the reaction, the organics continued to mineralize. From Fig. S7(b-f), SMT had converted to A and E firstly, and until they accumulated to a certain concentration, other small molecular products were produced. As shown in Fig. 9, cleavage occurred on the aromatic benzene and many carboxylic acids were produced (Liu and Wang, 2013; Boreen et al., 2004). The final mineralization of SMT was marked by the generation of CO_2 and H_2O , which was also confirmed by TOC analysis in this study.

3.5. Mechanism study

The mechanism inquiry is based on the characterization of the prepared composites and original biochar (Fig. 10), the information of free radicals obtained through quenching experiments and the analysis of the results of the intermediates obtained through LC-MS analysis. In previous studies, several methods has been applied to activate PS, including base, ultraviolet, heat, and mineral-based activators (Furman et al., 2010; He et al., 2014; Huang et al., 2005; Ahmad et al., 2010). The methods for activating PS in these studies are based on the exchange of electrons or the input of energy. In this study, Fe^{2+} released from FeMgO in water plays a major role in the activation progress and $\text{SO}_4^{\bullet-}$ is the main free radical in the process of SMT removal. Fig. 12b also indicated that Fe^{2+} partly converted to Fe^{3+} , which activated PS. The activation pathway of producing $\text{SO}_4^{\bullet-}$ could be summarized as the following approaches (Lee et al., 2009; Liang and Su, 2009; Liang et al., 2009) including Eq. (1), Eqs. (2) and (3). In addition, based on the superior adsorption capacity of MgFe_2O_4 and biochar, the activated $\text{SO}_4^{\bullet-}$ obtained opportunities for faster degradation of SMT.

In the process of producing Fe^{2+} , slow production speed will lead to a decrease in the efficiency of PS activation, but too fast production speed will lead to that $\text{S}_2\text{O}_8^{2-}$ reacts with excessive Fe^{2+} to form

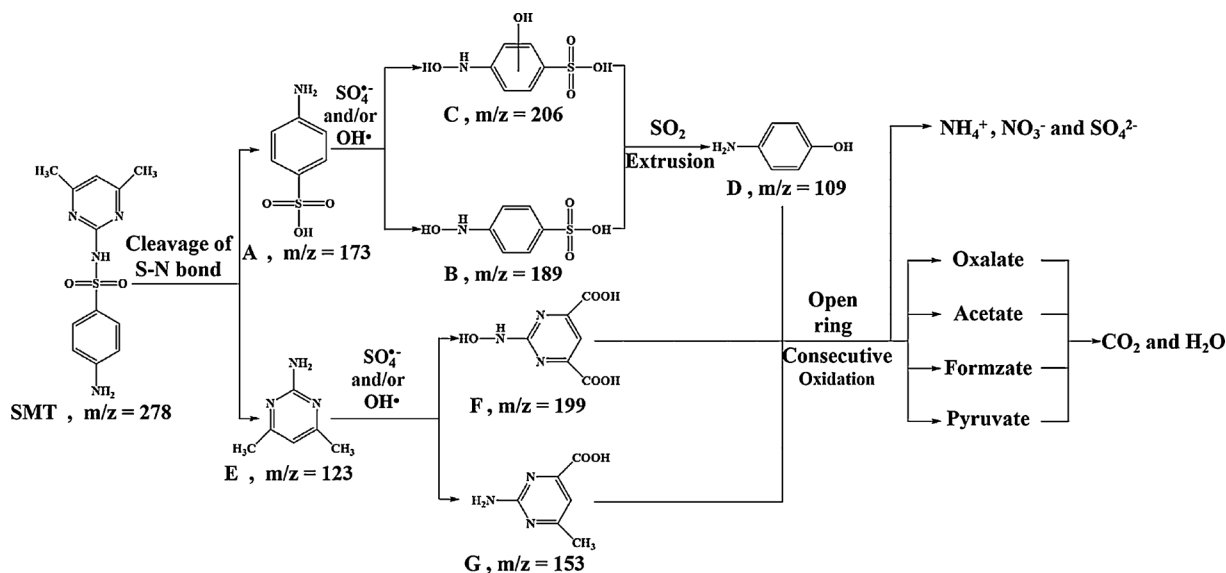
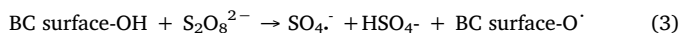
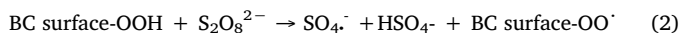
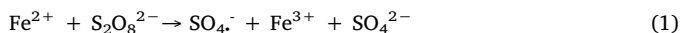


Fig. 9. SMT degradation pathway based on intermediates analysis by synergistical FeMgO/BC and PS process.

sulfate and can't react with the pollutants (Vicente et al., 2011). Combined with the three equations (Eqs. 1–3), which are also reflected in mechanism diagram (Fig. 10), biochar also acts as an activator. When the carboxyl and hydroxyl functional groups on the surface of biochar produce $\text{SO}_4^{\cdot-}$ as an electronic provider, these free radicals can reduce the pressure of adsorption because the $\text{SO}_4^{\cdot-}$ can play a role over a relatively wide area of liquid environment, not just the biochar surface (Matzek and Carter, 2016). The successful loading of FeMgO on biochar makes the production rate of $\text{SO}_4^{\cdot-}$ become appropriate and controllable.



3.6. Applications in natural waters

Five kinds of natural water samples were used in the experiment including running water (Changsha Running-water Company), Peach

lake (Changsha, China) water, Xiangjiang river (Changsha, China) water, Niuxin Pond water and Xichong Pond water. In particular, Peach lake water and Xiangjiang river water were sampled from three different sites for sampling to obtain more representative results. Deionized water was used as a control sample. It can be concluded from the experimental results (Fig. 11) that the removal amount of SMT in Xiangjiang river water was not significantly different from the removal rates in tap water and deionized water. And the content of TOC in flowing Xiangjiang river is lower, so the inferior removal rate in the other actual water bodies may be due to the reaction between natural organic matters and FeMgO/BC, which inhibits PS activation and reduces the amount of effective $\text{SO}_4^{\cdot-}$ (Cheng et al., 2019). Fig. 11 also shows that the removal rate of SMT was consistent with that of TOC. When the removal rate of SMT was high, the removal rate of TOC was relatively high. Besides, the existence of ions in the actual water may affect the effectiveness of the reaction. Wu et al. pointed out that Cl^- and HCO_3^- would react with $\text{SO}_4^{\cdot-}$ (Wu et al., 2018). Notably, the TOC removal rates of these natural water samples are all more than 50 %, especially, the rate of Xiangjiang river water sample is more than 62 %. The experiment shows that FeMgO/BC has the high efficiency in TOC and SMT removal in various actual waters. It can be inferred that the

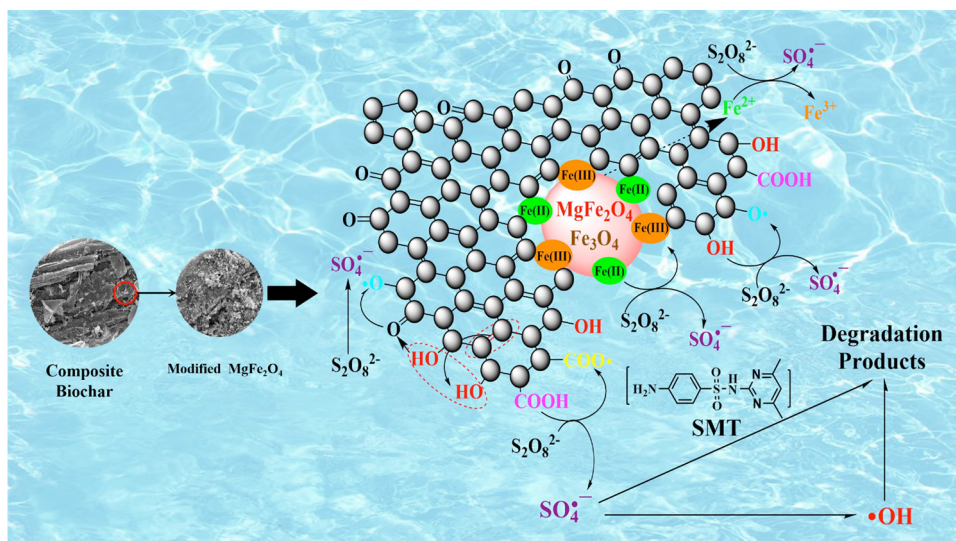


Fig. 10. Proposed mechanism and pathway of removing SMT in actual water bodies.

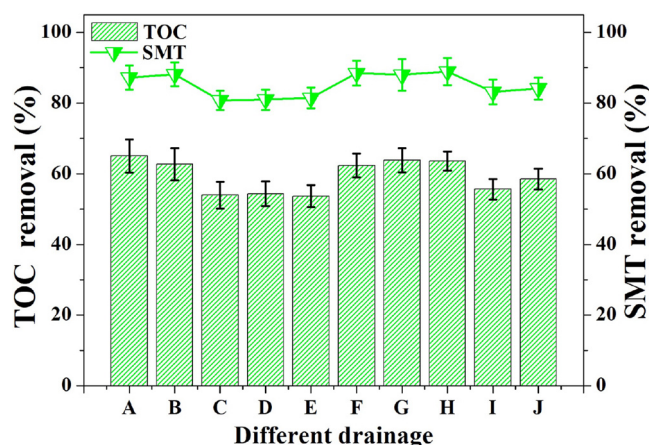


Fig. 11. Performance of $\text{MgFe}_2\text{O}_4/\text{BC}$ and TOC removal rate in real water.

FeMgO/BC could have many advantages of practical performance when applied in the actual waters.

3.7. Stability of FeMgO/BC

XPS characterizations of FeMgO/BC before and after reaction indicated the stability of FeMgO/BC . As shown in Fig. 12a, the surface element composition did not change significantly during the oxidation reaction. The XPS spectra of magnesium showed that only part Mg-C and $\text{Mg}(\text{OH})_2$ decreased in the reaction and the XPS spectra of iron changed slightly. Fig. S8 showed the leaching results of iron and magnesium during the reaction process. Obviously, the leaching rates of Fe and Mg were higher under acidic conditions. However, the leaching concentrations of iron in deionized water system, SMT/PS water system

and SMT water system were significantly lower than that of magnesium, and iron maintained a lower leaching rate under a wide range of pH conditions.

For the promotion and application of a composite, the cost is a vital consideration. The experimental data, shown in Fig. S8(a), indicated that the SMT removal amount of the system was still high after five times of repeated use. In particular, the removal efficiency at the fifth reuse only decreased 3.5 percent compared with the removal amount at the first use, and both had a fairly high level of performance. Considering the wide sources range and the low price of relevant raw materials for the preparation of FeMgO/BC , this material could be used as a stable and promising composite.

3.8. Toxicity analysis

The toxicity of reaction solution during treatment was also evaluated with traditional bacterial growth (gram-negative strain *E. coli*). As displayed in Fig. 13a, the inhibition rate of pure SMT solution (0 min) was more than 90 %, and the inhibition rate of SMT solution declined with the prolonging of the reaction time. The result indicated that the intermediate products of SMT degradation would be effectively removed and the toxicity enhancement towards bacteria was reduced. It was probably due to that SMT molecules degraded to some other products that were more biodegradable than the parent molecules. Generally, the higher degree of mineralization favored the reduction of toxicity to bacteria. Fig. 13b showed that the removal efficiency of TOC continuously increased with the improvement of SMT removal efficiency. At 30 min, the removal rates of SMT and TOC were 97.13 % and 77.89 %, respectively. Experiment results demonstrate that FeMgO/BC is eco-friendly for the removal of SMT in practical application.

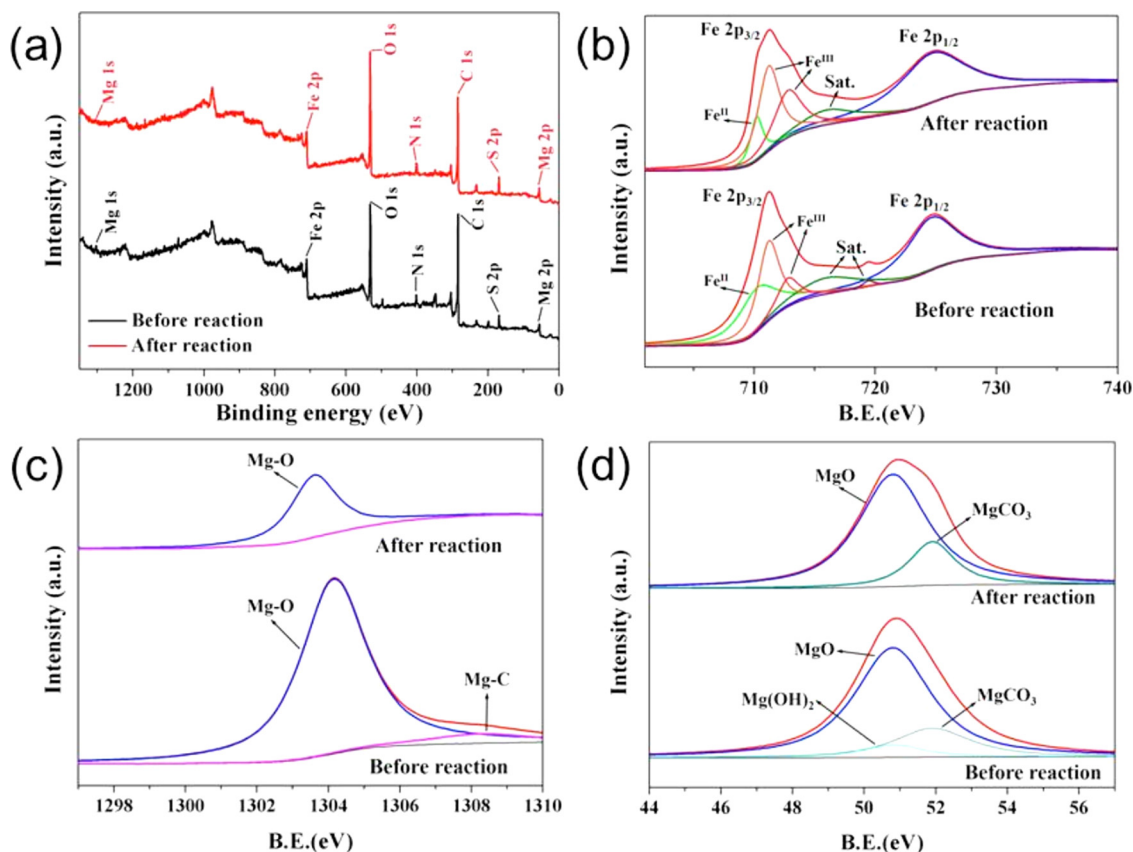


Fig. 12. XPS spectra (a) of FeMgO/BC before and after reaction. (b), (c) and (d) represent Fe 2p, Mg 2p and Mg 2s, respectively.

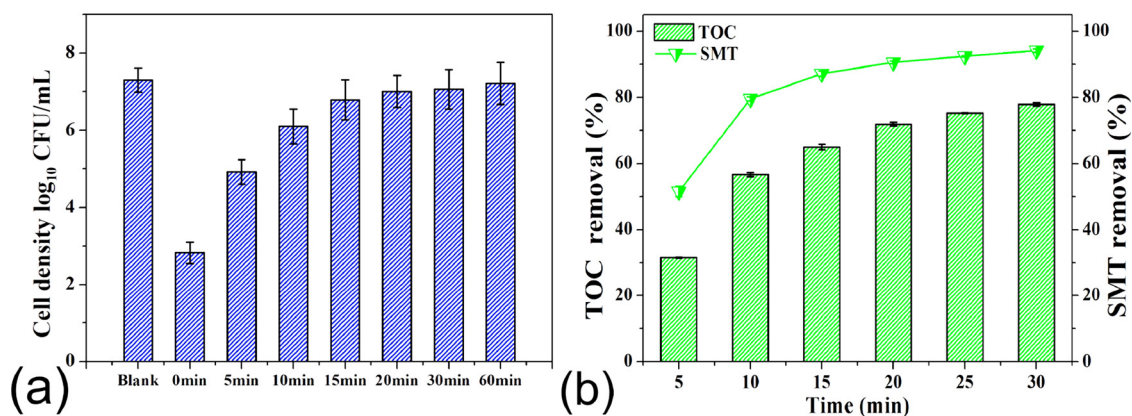


Fig. 13. (a) Evolution of solution (sampled during the reaction process) toxicity in terms of inhibition of *E. coli* growth. (b) The changes of SMT degradation and TOC removal during the reaction process.

4. Conclusions

In this study, maize straw derived biochar loaded with magnesium ferrite (FeMgO) has been successfully prepared, and is experimentally demonstrated to be effective on PS activation. A series of experiments have been conducted to investigate the influence of reaction conditions of FeMgO/BC in the removal of SMT. When the concentration of PS is 5 mM and the dosage of FeMgO/BC is 2 g/L, the removal rate of SMT in experimental water system can reach 99 % (pH = 3) and TOC removal efficiency reaches 77.9 %. The possible degradation pathways and the involved mechanism are proposed. MgFe₂O₄ could contribute to the magnetism and adsorption capacity, while the released Fe²⁺ from Fe₃O₄ performs well in the activation of S₂O₈²⁻. Functional groups on the surface of FeMgO/BC also provide effective binding sites for SMT, and carboxyl as well as hydroxyl on the surface can activate PS. Under a wide range of pH and in different practical water applications, SMT can be effectively removed by the synergistic reaction of FeMgO/BC and PS. The high TOC removal rate and the toxicity analysis results also proved the sustainability of the proposed composites. Moreover, FeMgO/BC is a new, promising and magnetic biochar-based composite for the SMT removal from actual water samples and contributes to dealing with the widely discussed problem of antibiotics removal in wastewater.

CRedit authorship contribution statement

Fanzhi Qin: Conceptualization, Methodology, Investigation, Data curation, Formal analysis. **Yijiao Peng:** Investigation, Writing - original draft, Data curation, Formal analysis. **Ge Song:** Investigation, Formal analysis. **Qingxuan Fang:** Investigation, Formal analysis. **Rongzhong Wang:** Conceptualization, Data curation, Methodology, Writing - review & editing. **Chen Zhang:** Conceptualization, Resources, Supervision, Project administration, Funding acquisition. **Guangming Zeng:** Supervision, Project administration, Funding acquisition. **Danlian Huang:** Supervision, Writing - review & editing. **Cui Lai:** Resources, Writing - review & editing. **Yaoyu Zhou:** Writing - review & editing. **Xiaofei Tan:** Writing - review & editing. **Min Cheng:** Writing - review & editing. **Shiyu Liu:** Writing - review & editing.

Declaration of Competing Interest

The authors declare that they have no known competing financial interests or personal relationships that could have appeared to influence the work reported in this paper.

Acknowledgements

This study was financially supported by the Program for the

National Natural Science Foundation of China (51809090, 51879101, 51579098, 51779090, 51709101, 51521006, 51909084), the Program for Changjiang Scholars and Innovative Research Team in University (IRT-13R17), the Three Gorges Follow-up Research Project (2017HXXY-05), the National Program for Support of Top-Notch Young Professionals of China (2014), the Fundamental Research Funds for the Central Universities, Hunan Provincial Science and Technology Plan Project (2018SK20410, 2017SK2243, 2016RS3026), the Program for New Century Excellent Talents in University (NCET-13-0186), the Natural Science Foundation of Hunan Province, China (Grant Nos. 2019JJ50077), and the Fundamental Research Funds for the Central Universities (531118010114, 531107050978, 541109060031).

Appendix A. Supplementary data

Supplementary material related to this article can be found, in the online version, at doi:<https://doi.org/10.1016/j.jhazmat.2020.122816>.

References

- Ahmad, M., Teel, A.L., Watts, R.J., 2010. Persulfate activation by subsurface minerals. *J. Contam. Hydrol.* 115, 34–45. <https://doi.org/10.1016/j.jconhyd.2010.04.002>.
- Ahmad, M., Rajapaksha, A.U., Lim, J.E., Zhang, M., Bolan, N., Mohan, D., Vithanage, M., Lee, S.S., Ok, Y.S., 2014. Biochar as a sorbent for contaminant management in soil and water: a review. *Chemosphere* 99, 19–33. <https://doi.org/10.1016/j.chemosphere.2013.10.071>.
- Barhoumi, N., Oturan, N., Olvera-Vargas, H., Brillas, E., Gadri, A., Ammar, S., Oturan, M.A., 2016. Pyrite as a sustainable catalyst in electro-Fenton process for improving oxidation of sulfamethazine. Kinetics, mechanism and toxicity assessment. *Water Res.* 94, 52–61. <https://doi.org/10.1016/j.watres.2016.02.042>.
- Boreen, A.L., Arnold, W.A., McNeill, K., 2004. Photochemical fate of sulfa drugs in the aquatic environment: sulfa drugs containing five-membered heterocyclic groups. *Environ. Sci. Technol.* 38, 3933–3940. <https://doi.org/10.1021/es0353053>.
- Bououdina, M., Alwqyan, T.S., Khezami, L., Al-Najar, B., Shaikh, M.N., Gill, R., Modwi, A., Taha, K.K., Lemine, O.M., 2019. Fabrication and characterization of nanostructured MgO-Fe₂O₃ composite by mechanical milling as efficient adsorbent of heavy metals. *J. Alloys. Compd.* 772, 1030–1039. <https://doi.org/10.1016/j.jallcom.2018.09.010>.
- Chen, B., Zhou, D., Zhu, L., 2008. Transitional adsorption and partition of Nonpolar and polar aromatic contaminants by biochars of pine needles with different pyrolytic temperatures. *Environ. Sci. Technol.* 42, 5137–5143. <https://doi.org/10.1021/es8002684>.
- Chen, H., Gao, B., Li, H., 2015. Removal of sulfamethoxazole and ciprofloxacin from aqueous solutions by graphene oxide. *J. Hazard. Mater.* 282, 201–207. <https://doi.org/10.1016/j.jhazmat.2014.03.063>.
- Chen, Y.-d., Ho, S.-H., Wang, D., Wei, Z.-s., Chang, J.-S., Ren, N.-q., 2018. Lead removal by a magnetic biochar derived from persulfate-ZVI treated sludge together with one-pot pyrolysis. *Bioresour. Technol.* 247, 463–470. <https://doi.org/10.1016/j.biortech.2017.09.125>.
- Cheng, M., Zeng, G., Huang, D., Lai, C., Liu, Y., Xu, P., Zhang, C., Wan, J., Hu, L., Xiong, W., Zhou, C., 2017. Salicylic acid-methanol modified steel converter slag as heterogeneous Fenton-like catalyst for enhanced degradation of alachlor. *Chem. Eng. J.* 327, 686–693. <https://doi.org/10.1016/j.cej.2017.06.153>.
- Cheng, M., Liu, Y., Huang, D., Lai, C., Zeng, G., Huang, J., Liu, Z., Zhang, C., Zhou, C., Qin, L., Xiong, W., Yi, H., Yang, Y., 2019. Prussian blue analogue derived magnetic Cu-Fe oxide as a recyclable photo-Fenton catalyst for the efficient removal of

- sulfamethazine at near neutral pH values. *Chem. Eng. J.* 362, 865–876. <https://doi.org/10.1016/j.cej.2019.01.101>.
- Furman, O.S., Teel, A.L., Watts, R.J., 2010. Mechanism of base activation of persulfate. *Environ. Sci. Technol.* 44, 6423–6428. <https://doi.org/10.1021/es1013714>.
- Gao, J., Pedersen, J.A., 2005. Adsorption of sulfonamide antimicrobial agents to clay minerals. *Environ. Sci. Technol.* 39, 9509–9516. <https://doi.org/10.1021/es050644c>.
- Gong, X., Huang, D., Liu, Y., Zeng, G., Wang, R., Wan, J., Zhang, C., Cheng, M., Qin, X., Xue, W., 2017. Stabilized nanoscale zerovalent iron mediated cadmium accumulation and oxidative damage of *Boehmeria nivea* (L.) Gaudich cultivated in cadmium contaminated sediments. *Environ. Sci. Technol.* 51, 11308–11316. <https://doi.org/10.1021/acs.est.7b03164>.
- Guo, X., Peng, Z., Huang, D., Xu, P., Zeng, G., Zhou, S., Gong, X., Cheng, M., Deng, R., Yi, H., Luo, H., Yan, X., Li, T., 2018. Biotransformation of cadmium-sulfamethazine combined pollutant in aqueous environments: phanerochaete chrysosporium bring cautious optimism. *Chem. Eng. J.* 347, 74–83. <https://doi.org/10.1016/j.cej.2018.04.089>.
- He, X., Mezyk, S.P., Michael, I., Fatta-Kassinos, D., Dionysiou, D.D., 2014. Degradation kinetics and mechanism of β -lactam antibiotics by the activation of H_2O_2 and $Na_2S_2O_8$ under UV-254nm irradiation. *J. Hazard. Mater.* 279, 375–383. <https://doi.org/10.1016/j.jhazmat.2014.07.008>.
- He, D., Zhang, C., Zeng, G., Yang, Y., Huang, D., Wang, L., Wang, H., 2019. A multi-functional platform by controlling of carbon nitride in the core-shell structure: from design to construction, and catalysis applications. *Appl. Catal. B* 117957. <https://doi.org/10.1016/j.apcatb.2019.117957>.
- Hu, C., Huang, D., Zeng, G., Cheng, M., Gong, X., Wang, R., Xue, W., Hu, Z., Liu, Y., 2018. The combination of Fenton process and *Phanerochaete chrysosporium* for the removal of bisphenol A in river sediments: mechanism related to extracellular enzyme, organic acid and iron. *Chem. Eng. J.* 338, 432–439. <https://doi.org/10.1016/j.cej.2018.01.068>.
- Huang, K.-C., Zhao, Z., Hoag, G.E., Dahmani, A., Block, P.A., 2005. Degradation of volatile organic compounds with thermally activated persulfate oxidation. *Chemosphere* 61, 551–560. <https://doi.org/10.1016/j.chemosphere.2005.02.032>.
- Huang, D., Wang, Y., Zhang, C., Zeng, G., Lai, C., Wan, J., Qin, L., Zeng, Y., 2016. Influence of morphological and chemical features of biochar on hydrogen peroxide activation: implications on sulfamethazine degradation. *RSC Adv.* 6, 73186–73196. <https://doi.org/10.1039/C6RA11850J>.
- Huang, D., Hu, C., Zeng, G., Cheng, M., Xu, P., Gong, X., Wang, R., Xue, W., 2017a. Combination of Fenton processes and biotreatment for wastewater treatment and soil remediation. *Sci. Total Environ.* 574, 1599–1610. <https://doi.org/10.1016/j.scitotenv.2016.08.199>.
- Huang, D., Liu, L., Zeng, G., Xu, P., Huang, C., Deng, L., Wang, R., Wan, J., 2017b. The effects of rice straw biochar on indigenous microbial community and enzymes activity in heavy metal-contaminated sediment. *Chemosphere* 174, 545–553. <https://doi.org/10.1016/j.chemosphere.2017.01.130>.
- Huang, D., Wang, X., Zhang, C., Zeng, G., Peng, Z., Zhou, J., Cheng, M., Wang, R., Hu, Z., Qin, X., 2017c. Sorptive removal of ionizable sulfamethazine from aqueous solution by graphene oxide-coated biochar nanocomposites: influencing factors and mechanism. *Chemosphere* 186, 414–421. <https://doi.org/10.1016/j.chemosphere.2017.07.154>.
- Huang, D., Luo, H., Zhang, C., Zeng, G., Lai, C., Cheng, M., Wang, R., Deng, R., Xue, W., Gong, X., Guo, X., Li, T., 2019. Nonnegligible role of biomass types and its compositions on the formation of persistent free radicals in biochar: Insight into the influences on Fenton-like process. *Chem. Eng. J.* 361, 353–363. <https://doi.org/10.1016/j.cej.2018.12.098>.
- Jung, K.-W., Ahn, K.-H., 2016. Fabrication of porosity-enhanced MgO/biochar for removal of phosphate from aqueous solution: application of a novel combined electrochemical modification method. *Bioresour. Technol.* 200, 1029–1032. <https://doi.org/10.1016/j.biortech.2015.10.008>.
- Jung, K.W., Lee, S., Lee, Y.J., 2017. Synthesis of novel magnesium ferrite (MgFe₂O₄)/biochar magnetic composites and its adsorption behavior for phosphate in aqueous solutions. *Bioresour. Technol.* 245, 751–759. <https://doi.org/10.1016/j.biortech.2017.09.035>.
- Khot, V.M., Salunkhe, A.B., Phadate, M.R., Pawar, S.H., 2012. Formation, microstructure and magnetic properties of nanocrystalline MgFe₂O₄. *Mater. Chem. Phys.* 132, 782–787. <https://doi.org/10.1016/j.matchemphys.2011.12.012>.
- Kohsari, H.K., Norouzbeigi, R., 2018. Impregnated active layer combustion synthesis of nano MgFe₂O₄ using green template. *Ceram. Int.* 44, 19227–19235. <https://doi.org/10.1016/j.ceramint.2018.07.147>.
- Lai, C., Liu, S., Zhang, C., Zeng, G., Huang, D., Qin, L., Liu, X., Yi, H., Wang, R., Huang, F., Li, B., Hu, T., 2018. Electrochemical aptasensor based on sulfur-Nitrogen codoped ordered mesoporous carbon and thymine-Hg²⁺-Thymine mismatch structure for Hg²⁺ detection. *ACS Sens.* 3, 2566–2573. <https://doi.org/10.1021/acssensors.8b00926>.
- Lan, Y., Coetsier, C., Causserand, C., Groenen Serrano, K., 2018. An experimental and modelling study of the electrochemical oxidation of pharmaceuticals using a boron-doped diamond anode. *Chem. Eng. J.* 333, 486–494. <https://doi.org/10.1016/j.cej.2017.09.164>.
- Lau, T.K., Chu, W., Graham, N.J.D., 2007. The aqueous degradation of butylated hydroxyanisole by UV/S₂O₈²⁻: study of reaction mechanisms via dimerization and mineralization. *Environ. Sci. Technol.* 41, 613–619. <https://doi.org/10.1021/es061395a>.
- Lee, Y.-C., Lo, S.-L., Chiueh, P.-T., Chang, D.-G., 2009. Efficient decomposition of perfluorocarboxylic acids in aqueous solution using microwave-induced persulfate. *Water Res.* 43, 2811–2816. <https://doi.org/10.1016/j.watres.2009.03.052>.
- Li, B., Li, L., Lin, K., Zhang, W., Lu, S., Luo, Q., 2013. Removal of 1,1,1-trichloroethane from aqueous solution by a sono-activated persulfate process. *Ultrason. Sonochem.* 20, 855–863. <https://doi.org/10.1016/j.ultrsonch.2012.11.014>.
- Li, R., Wang, J.J., Zhou, B., Awasthi, M.K., Ali, A., Zhang, Z., Gaston, L.A., Lahori, A.H., Mahar, A., 2016. Enhancing phosphate adsorption by Mg/Al layered double hydroxide functionalized biochar with different Mg/Al ratios. *Sci. Total Environ.* 559, 121–129. <https://doi.org/10.1016/j.scitotenv.2016.03.151>.
- Liang, C., Su, H.-W., 2009. Identification of sulfate and hydroxyl radicals in thermally activated persulfate. *Ind. Eng. Chem. Res.* 48, 5558–5562. <https://doi.org/10.1021/ie9002848>.
- Liang, C., Bruell, C.J., Marley, M.C., Sperry, K.L., 2004. Persulfate oxidation in situ remediation of TCE. I. Activated by ferrous ion with and without a persulfate-thiosulfate redox couple. *Chemosphere* 55, 1213–1223. <https://doi.org/10.1016/j.chemosphere.2004.01.029>.
- Liang, C., Lin, Y.-T., Shih, W.-H., 2009. Treatment of trichloroethylene by adsorption and persulfate oxidation in batch studies. *Ind. Eng. Chem. Res.* 48, 8373–8380. <https://doi.org/10.1021/ie900841k>.
- Lin, H., Wu, J., Oturan, N., Zhang, H., Oturan, M.A., 2016. Degradation of artificial sweetener saccharin in aqueous medium by electrochemically generated hydroxyl radicals. *Environ. Sci. Pollut. Res. - Int.* 23, 4442–4453. <https://doi.org/10.1007/s11356-015-5633-x>.
- Ling, C., Li, X., Zhang, Z., Liu, F., Deng, Y., Zhang, X., Li, A., He, L., Xing, B., 2016. High adsorption of sulfamethoxazole by an amine-modified polystyrene-divinylbenzene resin and its mechanistic insight. *Environ. Sci. Technol.* 50, 10015–10023. <https://doi.org/10.1021/acs.est.6b02846>.
- Liu, Y., Wang, J., 2013. Degradation of sulfamethazine by gamma irradiation in the presence of hydrogen peroxide. *J. Hazard. Mater.* 250–251, 99–105. <https://doi.org/10.1016/j.jhazmat.2013.01.050>.
- Matzek, L.W., Carter, K.E., 2016. Activated persulfate for organic chemical degradation: a review. *Chemosphere* 151, 178–188. <https://doi.org/10.1016/j.chemosphere.2016.02.055>.
- Mohammadi, N., Khani, H., Gupta, V.K., Amereh, E., Agarwal, S., 2011. Adsorption process of methyl orange dye onto mesoporous carbon material-kinetic and thermodynamic studies. *J. Colloid Interface Sci.* 362, 457–462. <https://doi.org/10.1016/j.jcis.2011.06.067>.
- Muhamad, S., Shukla, P.R., Tádé, M.O., Wang, S., 2012. Heterogeneous activation of peroxymonosulphate by supported ruthenium catalysts for phenol degradation in water. *J. Hazard. Mater.* 215–216, 183–190. <https://doi.org/10.1016/j.jhazmat.2012.02.045>.
- Sun, P., Li, Y., Meng, T., Zhang, R., Song, M., Ren, J., 2018. Removal of sulfonamide antibiotics and human metabolite by biochar and biochar/H₂O₂ in synthetic urine. *Water Res.* 147 (15), 91–100. <https://doi.org/10.1016/j.watres.2018.09.051>.
- Tang, W., Su, Y., Li, Q., Gao, S., Shang, J.K., 2013. Superparamagnetic magnesium ferrite nano-adsorbent for effective arsenic (III, V) removal and easy magnetic separation. *Water Res.* 47, 3624–3634. <https://doi.org/10.1016/j.watres.2013.04.023>.
- Teixidó, M., Pignatello, J.J., Beltrán, J.L., Granados, M., Peccia, J., 2011. Speciation of the ionizable antibiotic sulfamethazine on black carbon (Biochar). *Environ. Sci. Technol.* 45, 10020–10027. <https://doi.org/10.1021/es202487h>.
- Tian, S., Zhang, C., Huang, D., Wang, R., Zeng, G., Yan, M., Xiong, W., Zhou, C., Cheng, M., Xue, W., 2019. Recent progress in sustainable technologies for adsorptive and reactive removal of sulfonamides. *Chem. Eng. J.* 123423. <https://doi.org/10.1016/j.cej.2019.123423>.
- Vicente, F., Santos, A., Romero, A., Rodriguez, S., 2011. Kinetic study of diuron oxidation and mineralization by persulphate: effects of temperature, oxidant concentration and iron dosage method. *Chem. Eng. J.* 170, 127–135. <https://doi.org/10.1016/j.cej.2011.03.042>.
- Wacławek, S., Antoš, V., Hrabák, P., Černík, M., 2016. Remediation of hexachlorocyclohexanes by cobalt-mediated activation of peroxymonosulfate. *Desalination*. *Water Treat.* 57, 26274–26279. <https://doi.org/10.1080/19443994.2015.1119757>.
- Wang, J., Liao, Z., Iftikhar, J., Shi, L., Du, Y., Zhu, J., Xi, S., Chen, Z., Chen, Z., 2017. Treatment of refractory contaminants by sludge-derived biochar/persulfate system via both adsorption and advanced oxidation process. *Chemosphere* 185, 754–763. <https://doi.org/10.1016/j.chemosphere.2017.07.084>.
- Wang, W., Xu, P., Chen, M., Zeng, G., Zhang, C., Zhou, C., Yang, Y., Huang, D., Lai, C., Cheng, M., Hu, L., Xiong, W., Guo, H., Zhou, M., 2018. Alkali metal-assisted synthesis of graphite carbon nitride with tunable band-gap for enhanced visible-light-driven photocatalytic performance. *ACS Sustain. Chem. Eng.* 6, 15503–15516. <https://doi.org/10.1021/acssuschemeng.8b03965>.
- Wu, S., He, H., Li, X., Yang, C., Zeng, G., Wu, B., He, S., Lu, L., 2018. Insights into atrazine degradation by persulfate activation using composite of nanoscale zero-valent iron and graphene: performances and mechanisms. *Chem. Eng. J.* 341, 126–136. <https://doi.org/10.1016/j.cej.2018.01.136>.
- Xiao, F., Li, W., Fang, L., Wang, D., 2016. Synthesis of akaganeite (beta-FeOOH)/reduced graphene oxide nanocomposites for oxidative decomposition of 2-chlorophenol by Fenton-like reaction. *J. Hazard. Mater.* 308, 11–20. <https://doi.org/10.1016/j.jhazmat.2016.01.011>.
- Yan, J., Gao, W., Dong, M., Han, L., Qian, L., Nathanail, C.P., Chen, M., 2016. Degradation of trichloroethylene by activated persulfate using a reduced graphene oxide supported magnetite nanoparticle. *Chem. Eng. J.* 295, 309–316. <https://doi.org/10.1016/j.cej.2016.01.085>.
- Yang, Y., Sheng, G., 2003. Pesticide adsorptivity of aged particulate matter arising from crop residue burns. *J. Agric. Food Chem.* 51, 5047–5051. <https://doi.org/10.1021/jf0345301>.
- Yang, Y., Zeng, Z., Zhang, C., Huang, D., Zeng, G., Xiao, R., Lai, C., Zhou, C., Guo, H., Xue, W., Cheng, M., Wang, W., Wang, J., 2018. Construction of iodine vacancy-rich BiO/Ag@AgI z-scheme heterojunction photocatalysts for visible-light-driven tetracycline degradation: transformation pathways and mechanism insight. *Chem. Eng. J.* 349,

- 808–821. <https://doi.org/10.1016/j.cej.2018.05.093>.
- Yang, Y., Zhang, C., Huang, D., Zeng, G., Huang, J., Lai, C., Zhou, C., Wang, W., Guo, H., Xue, W., 2019a. Boron nitride quantum dots decorated ultrathin porous g-C₃N₄: intensified exciton dissociation and charge transfer for promoting visible-light-driven molecular oxygen activation. *Appl. Catal. B* 245, 87–99. <https://doi.org/10.1016/j.apcatb.2018.12.049>.
- Yang, Y., Zeng, Z., Zeng, G., Huang, D., Xiao, R., Zhang, C., Zhou, C., Xiong, W., Wang, W., Cheng, M., 2019b. Ti₃C₂ MXene/porous g-C₃N₄ interfacial Schottky junction for boosting spatial charge separation in photocatalytic H₂O₂ production. *Appl. Catal. B* 258, 117956. <https://doi.org/10.1016/j.apcatb.2019.117956>.
- Yao, Y., Gao, B., Chen, J., Yang, L., 2013. Engineered biochar reclaiming phosphate from aqueous solutions: mechanisms and potential application as a slow-release fertilizer. *Environ. Sci. Technol.* 47, 8700–8708. <https://doi.org/10.1021/es4012977>.
- Yin, R., Guo, W., Wang, H., Du, J., Wu, Q., Chang, J.-S., Ren, N., 2019. Singlet oxygen-dominated peroxydisulfate activation by sludge-derived biochar for sulfamethoxazole degradation through a nonradical oxidation pathway: Performance and mechanism. *Chem. Eng. J.* 357, 589–599. <https://doi.org/10.1016/j.cej.2018.09.184>.
- Zeng, T., Zhang, X., Wang, S., Niu, H., Cai, Y., 2015. Spatial confinement of a Co₃O₄ catalyst in hollow metal-organic frameworks as a nanoreactor for improved degradation of organic pollutants. *Environ. Sci. Technol.* 49, 2350–2357. <https://doi.org/10.1021/es505014z>.
- Zhang, W., Zhou, C., Zhou, W., Lei, A., Zhang, Q., Wan, Q., Zou, B., 2011. Fast and considerable adsorption of methylene blue dye onto graphene oxide. *Bull. Environ. Contam. Toxicol.* 87, 86. <https://doi.org/10.1007/s00128-011-0304-1>.
- Zhang, M., Gao, B., Yao, Y., Xue, Y., Inyang, M., 2012. Synthesis of porous MgO-biochar nanocomposites for removal of phosphate and nitrate from aqueous solutions. *Chem. Eng. J.* 210, 26–32. <https://doi.org/10.1016/j.cej.2012.08.052>.
- Zhang, C., Lai, C., Zeng, G., Huang, D., Yang, C., Wang, Y., Zhou, Y., Cheng, M., 2016. Efficacy of carbonaceous nanocomposites for sorbing ionizable antibiotic sulfamethazine from aqueous solution. *Water Res.* 95, 103–112. <https://doi.org/10.1016/j.watres.2016.03.014>.
- Zhang, H., Xue, G., Chen, H., Li, X., 2018. Magnetic biochar catalyst derived from biological sludge and ferric sludge using hydrothermal carbonization: preparation, characterization and its circulation in Fenton process for dyeing wastewater treatment. *Chemosphere* 191, 64–71. <https://doi.org/10.1016/j.chemosphere.2017.10.026>.
- Zhang, C., Wang, W., Duan, A., Zeng, G., Huang, D., Lai, C., Tan, X., Cheng, M., Wang, R., Zhou, C., Xiong, W., Yang, Y., 2019a. Adsorption behavior of engineered carbons and carbon nanomaterials for metal endocrine disruptors: experiments and theoretical calculation. *Chemosphere* 222, 184–194. <https://doi.org/10.1016/j.chemosphere.2019.01.128>.
- Zhang, C., Zeng, G., Huang, D., Lai, C., Chen, M., Cheng, M., Tang, W., Tang, L., Dong, H., Huang, B., 2019b. Biochar for environmental management: mitigating greenhouse gas emissions, contaminant treatment, and potential negative impacts. *Chem. Eng. J.* 373 (1), 902–922. <https://doi.org/10.1016/j.cej.2019.05.139>.
- Zhou, J., Song, H., Ma, L., Chen, X., 2011. Magnetite/graphene nanosheet composites: interfacial interaction and its impact on the durable high-rate performance in lithium-ion batteries. *RSC Adv.* 1, 782–791. <https://doi.org/10.1039/C1RA00402F>.
- Zhou, T., Wu, X., Mao, J., Zhang, Y., Lim, T.-T., 2014. Rapid degradation of sulfonamides in a novel heterogeneous sonophotocatalytic magnetite-catalyzed Fenton-like (US/UV/Fe₃O₄/oxalate) system. *Appl. Catal. B* 160–161, 325–334. <https://doi.org/10.1016/j.apcatb.2014.05.036>.
- Zhou, X., Lai, C., Huang, D., Zeng, G., Chen, L., Qin, L., Xu, P., Cheng, M., Huang, C., Zhang, C., Zhou, C., 2018. Preparation of water-compatible molecularly imprinted thiol-functionalized activated titanium dioxide: selective adsorption and efficient photodegradation of 2, 4-dinitrophenol in aqueous solution. *J. Hazard. Mater.* 346, 113–123. <https://doi.org/10.1016/j.jhazmat.2017.12.032>.